RSC Advances

PAPER

View Article Online
View Journal | View Issue

Cite this: *RSC Adv.*, 2022, **12**, 15584

Bioinspired nacre-like PEEK material with superior tensile strength and impact toughness†

Shu Zhu,[ab] Tianwen Yan,[ab] Xinlin Huang,[ab] Elwathig A. M. Hassan,[abd] Jianfeng Zhou,*[ab] Sen Zhang,[ac] Mengyun Xiong,[ab] Muhuo Yu[ab] and Zhaomin Li[e]

A bioinspired PEEK material with hard "bricks" of nanoscale lamellae and micron-scale deformed spherulites bonded by soft "mortar" of a rigid amorphous fraction was produced with a pressure-induced flow (PIF) processing applied in the solid-state. Novel mechanisms were proposed for the marked and simultaneous improvement in the strength and toughness, where the tensile strength and impact strength could be increased to ~200% and ~450%, respectively. On one hand, the rotation, recombination and restacking of the crystalline blocks formed an oriented and stratified morphology similar to the "brick-and-mortar" structure in nacre, and resulted in the confined crack propagations and the tortuous energy dissipating paths. On the other hand, the PIF-relaxation due to the newly generated rigid amorphous fraction further contributed to the improvement of the impact strength. The efficiency of enhancement could be controlled by the molding temperature, the compression ratio, and the volume fraction of chopped carbon fiber. As a result, PIF-processing might endow the PEEK material with improved mechanical matching with the surrounding tissues and extended service life in biomedical applications while retaining excellent biocompatibility with no external substances introduced.

Received 13th February 2022
Accepted 12th May 2022

DOI: 10.1039/d2ra00667g

rsc.li/rsc-advances

1. Introduction

Polyetheretherketone (PEEK) is a well-known high-performance thermoplastic polymer with attractive properties, such as good chemical resistance, high mechanical properties, excellent friction resistance, high thermal stability and excellent electrical performance.[1,2] The interest in PEEK and carbon fiber reinforced (CFR) PEEK in the context of biomedical engineering lies with the proven inertness of the polymer in many aggressive environments and the potential to control the elastic modulus of the composites such that biomechanical compatibility with bone might be achieved.[3–5] Although neat (unfilled) PEEK can exhibit an elastic modulus ranging from 3 to 4 GPa, the modulus can be tailored to closely match cortical bone (18 GPa) or titanium alloy (110 GPa) by preparing carbon-fiber-reinforced composites with varying fiber length and orientation.[6,7] Therefore, PEEK and its composites have already been broadly accepted as a radiolucent alternative to metallic biomaterials in clinical applications such as dental, trauma, orthopedic, and spinal implants.[8–11]

However, merely adjusting the type and concentration of fiber is not able to solve all the problems while designing those implants. There are two paradoxical relations that must be carefully dealt with: (1) the trade-off between mechanical performance and biological compatibility.[12,13] Many load-bearing implants require materials with a strength comparable to that of metals, which demands a large volume fraction of fiber reinforcement; however, the presence of these fibers at the surface may adversely affect biocompatibility. (2) The conflict lies between the strength and the toughness (durability).[14] Unfilled PEEK offers ductility, good impact resistance and isotropic properties but often lacks sufficient stiffness and strength, while reinforced PEEK grades are typically the opposite – very strong and stiff materials but comparatively brittle.[15,16]

Nacre makes a perfect example material in nature that shows ultra-high strength and toughness at the same time.[17–19] Natural seashell nacre consists of approximately 95% aragonite (a mineral form of $CaCO_3$) and a few percent of biological macromolecules; yet its impact strength is 3000 folds of its mineral constituency.[20] The superior strength and toughness of

[a]*State Key Laboratory for Modification of Chemical Fibers and Polymer Materials, Shanghai Collaborative Innovation Center of High-Performance Fibers and Composites (Province-Ministry Joint), Key Laboratory of High-Performance Fibers & Products, Ministry of Education, Center for Civil Aviation Composites, Donghua University, Shanghai, 201620, P. R. China. E-mail: zjf@dhu.edu.cn*

[b]*Key Laboratory of Shanghai City for Lightweight Composites, College of Materials Science and Engineering, Donghua University, Shanghai, 201620, P. R. China*

[c]*Liaoning Engineering Technology Research Center of Function Fiber and Its Composites, Dalian Polytechnic University, Dalian 116034, China*

[d]*Industries Engineering and Technology, University of Gezira, Sudan*

[e]*Shanghai Microport Medical (Group) Co. Ltd, Shanghai 201203, China*

† Electronic supplementary information (ESI) available: Table S1: compression ratio of samples during PIF-processing as functions of temperature and pressure. Fig. S1: SEM images of fractured surfaces after impact tests for PEEK samples: (a) and (b) without PIF-processing; (c) and (d) after PIF-processing. See https://doi.org/10.1039/d2ra00667g

seashell nacre are attributed to the robust nanostructure in which the protein collagen layers (10–50 nm thick) and aragonite platelets (200–900 nm thick) form an ordered "brick-and-mortar" structure, where the brick (platelet) interlocks allow a large amount of fracture energy to dissipate in the mortar (protein) *via* shear deformation.[17,21] Some ultra-tough and ultra-strong nacre-inspired materials have been made through strict methods, such as layer-by-layer, self-assembly, and freeze-casting.[22–27] However, generating microscopically stratified structures mainly containing lightweight materials such as polymers, which at the same time are uniformly aligned on a large length scale (*e.g.*, in bulk material), has turned out to be difficult.[28,29]

In this study, we prepared a nacre-like PEEK material with superior tensile strength and toughness through a method of pressure-induced flow (PIF) that we developed,[30] and proposed more comprehensive mechanisms for the simultaneous strengthening and toughening. We revealed that during PIF-processing performed at processing temperatures below the melting point, the hard domains (crystalline lamellae) retained their integrity but were aligned in the flow field to form an oriented and stratified morphology among the soft domains of the amorphous region to simultaneously boost the toughness and strength. The validity and efficiency for enhancing PEEK samples were confirmed by characterizations on the mechanical performances, crystallization and orientation behaviors, and fracture surface morphologies with different techniques, such as tensile stress–strain curves, differential scanning calorimetry, two-dimensional X-ray diffraction, and scanning electron microscopy. With a unique combination of high stiffness and excellent ductility, the PIF-processed PEEK bridges the performance gap between unfilled PEEK and traditional CFR PEEK grades, and the method provided in this work can also be used in guiding the design of other structural materials.

2. Materials and methods

Materials

Polyetheretherketone (PEEK) (Type 7500G) was supplied by Jiangsu Junhua High Performance Specialty Engineering Plastics (PEEK) Products Co., Ltd. The M_w of PEEK was ~150 000. Acetone (≥99.5%) was supplied by Shanghai Yunli Economic and Trading Co., Ltd.

Sample preparations

PEEK powder was dried in a vacuum oven at 100 °C for 24 h and then injected at 390 °C under 10 MPa into a mold (80 mm × 10 mm × 4 mm) at room temperature. The injected PEEK specimens were cleaned with acetone and then dried in a vacuum oven at 220 °C for 2 h to crystallize completely. After treatments, the PEEK samples were placed in a die designed for PIF-processing[31] (as shown in Fig. 1) and preheated for 15 min at the desired temperature to achieve an equilibrium of temperature for the samples and the die. PIF-processing was conducted with a press (XLB-D/S, Shanghai Dehong Rubber & Plastic Machinery Co., Ltd) under certain pressures for 5 min. LD, FD and CD represent the loading direction, flowing direction and constraint direction, respectively.

In order to quantitatively characterize the size changes of PEEK samples, we defined the ratio of respective thicknesses before and after PIF-processing as the compression ratio, expressed by R:

$$R = d_1/d_2 \quad (1)$$

where d_1 and d_2 are the thicknesses before and after PIF-processing, respectively. By changing the molding pressure at 280 °C, samples with compression ratios of 1.0, 1.4, 1.6, 1.8, 2.2 and 2.6 were obtained. In addition, PEEK samples with a compression ratio of approximately 1.7 were obtained at different PIF molding temperatures, with a pair of metal gaskets as the auxiliary positioning support, to evaluate the influence of the molding temperature on PIF-processing. The correspondence between compression ratio and molding pressure was listed in Table S1 in the ESI.†

Tensile test

The tensile tests were performed according to ISO 527-1:1993 with a universal testing machine (Model 5566, Shanghai Xieqiang Instrument Manufacturing Co., Ltd) at room temperature and a stretching speed of 50 mm min^{-1} along FD. Each result represents the average value from 5 parallel tests, with an error bar calculated as the mean square error of the 5 results. The tensile strength of the samples was defined as the maximum value of strength in a stress–strain curve and calculated as

$$\sigma = P/(b \times d) \quad (2)$$

where σ is the tensile strength of the sample (MPa), P is the maximum value of force (N), b is the width of the sample (mm), and d is the thickness of the sample (mm). The elongation at break was the maximum elongation in the stress–strain curve before a steep drop of stress.

Impact test

Impact testing was used to investigate the behavior of samples under specific impact conditions and to estimate their toughness within the limitations inherent to the test conditions.

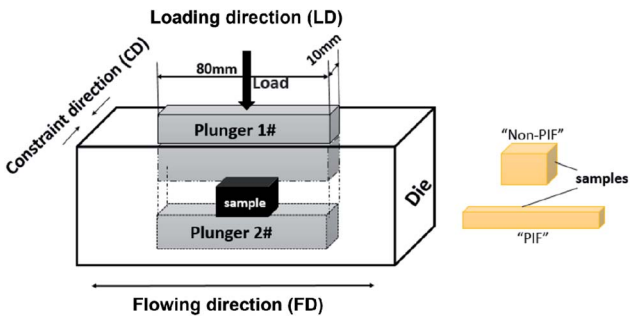

Fig. 1 Schematic drawing of the die and samples for pressure-induced flow (PIF) processing.

Pendulum geometry may use a cantilever support as in Notched Izod impact testing (ISO 180:2000); the impact strengths were measured using a CEAST Resil Impactor (Italy) at an impact rate of 3.46 m s^{-1}.

Differential scanning calorimeter (DSC)

The DSC curves of samples with non-PIF or PIF were obtained in a TA-Q20 differential scanning calorimeter (TA Instrument Company, USA). The sample mass for DSC measurement was approximately 5–10 mg. The experiment was carried out in the temperature range from 40 to 395 °C, with a scanning rate of 10 °C min^{-1} under a nitrogen atmosphere.

Dynamic mechanical analysis (DMA)

The thermomechanical properties of PEEK samples were measured using a Q800 dynamic mechanical analyzer (TA Instrument Company, USA) at a heating rate of 3 °C min^{-1} and a frequency of 1 Hz within the temperature range from 100 °C to 325 °C. A single cantilever bending mode was used, and the amplitude of deformation was set at 15 μm. The sinusoidal force was applied to each sample along LD.

X-ray diffraction (XRD)

The data for the crystalline portion of PEEK samples were collected using an X-ray diffractometer (D8 Discover, Bruker, Germany). The X-ray irradiation of Cu-α with a wavelength of 1.54 Å hits the sample along the CD and LD under a tube voltage of 40 kV and electric current of 40 mA for 60 s, respectively.

Scanning electron microscopy (SEM) analysis

The PEEK samples after impact and tensile tests, with and without PIF-processing (with a compression ratio of 1.8), were observed by scanning electron microscopy (Quanta 250, Thermo Fisher Scientific, USA) to investigate the fracture surface morphologies, with an accelerating voltage of 12.50 kV. Surfaces are pretreated by gold sputtering.

3. Results and discussion

The tensile strength and impact strength for PEEK could be markedly and simultaneously improved after PIF-processing. As shown in Fig. 2A, the tensile strength exhibited a characteristic "S" shape increase with increasing compression ratios. It first gradually increased at small compression ratios, rapidly increased with larger compression ratios, and then gently increased after a compression ratio of 2.2. The maximum strength under a compression ratio of 2.6 amounted to ~2 folds of the non-PIF sample. The notched Izod impact strength, reflecting the toughness, quickly increased with increasing compression ratio. However, when the compression ratio was larger than 2.2, the impact strength increased gently or even decreased. The maximum increase occurred under a compression ratio between 1.7 and 2.2, where the impact strength after PIF-processing reached above 35 kJ cm^{-2}, showing an enhancement of ~450% (the average impact strength for non-PIF PEEK was 7.9 kJ cm^{-2}). This simultaneous improvement of impact strength and tensile strength seems novel for this kind of high performance polymers, where toughness improvements are generally at the cost of unsatisfactory tensile properties,[28] and *vice versa*.[32]

Fig. 2B presents the stress–strain curves for tensile tests. Both the tensile strength and elongation at break of PEEK after PIF-processing were much higher than those of non-PIF samples. Interestingly, for all PIF-processed samples, an inflection occurred near the inherent yield stress of the corresponding non-PIF sample, while no real yield behavior occurred at this point, and a "second yield" point occurred at a tensile stress much higher than the original yielding strength (except for the sample with the highest compression ratio of 2.6). It is right the "second yield" that causes a much higher elongation at break and therefore higher yield strength and tensile strength, which is distinct from the conventional style of strengthening by improving the moduli.

Beyond the traditional yield point, the tensile stress for the non-PIF sample rapidly decreased until the complete disentanglement and mutual slippage of molecular chains took place in certain places of the continuous phase of amorphous

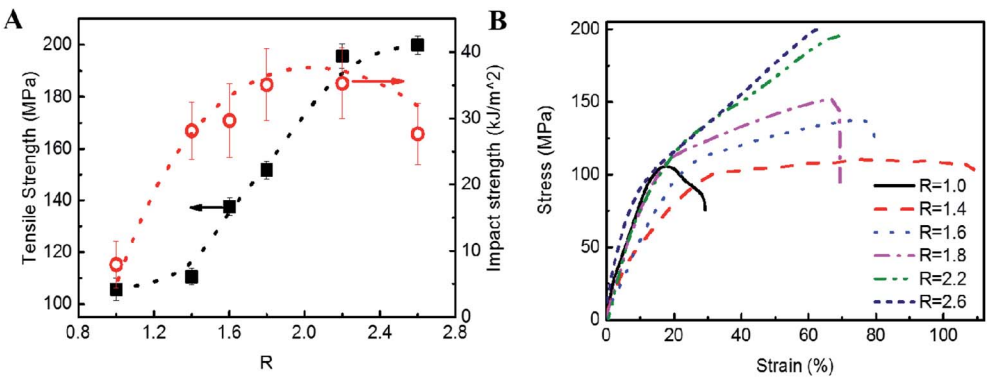

Fig. 2 (A) Tensile strength and fracture toughness of PEEK samples with different compression ratios. (B) Stress–strain curves of PEEK samples with different compression ratios at 280 °C.

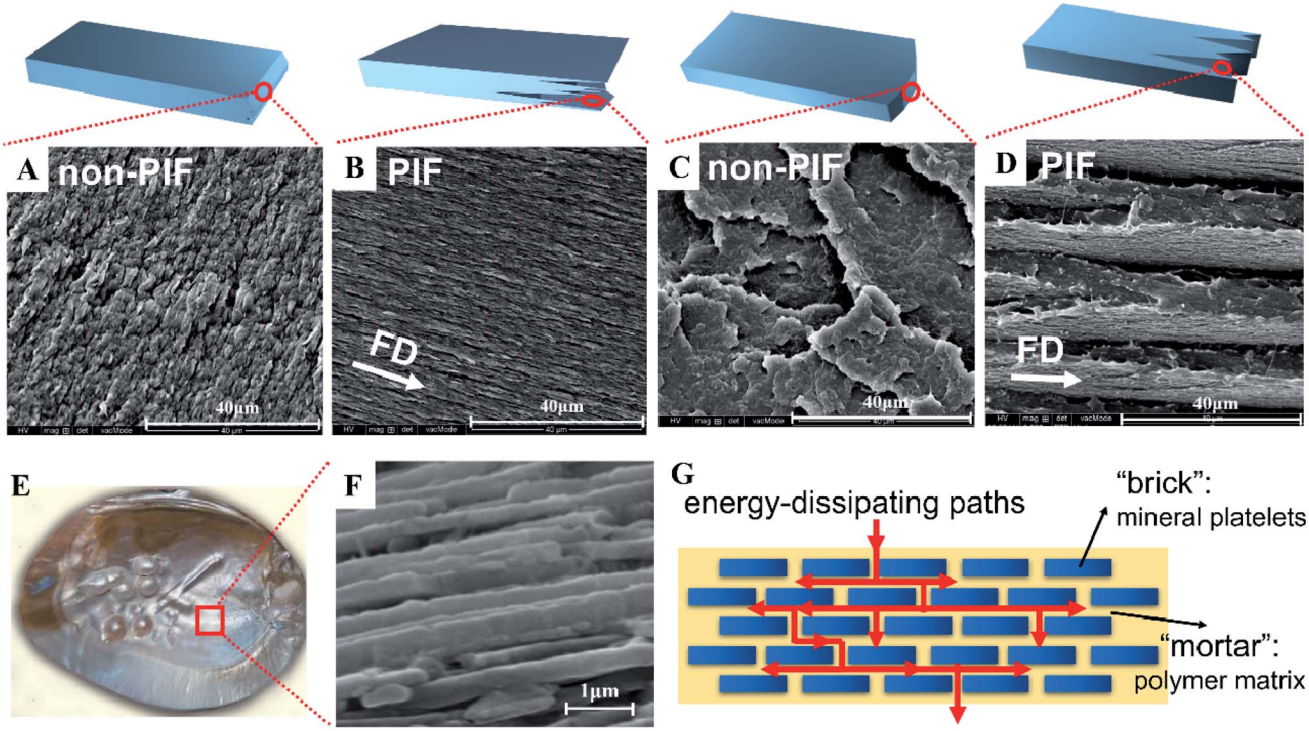

Fig. 3 SEM images of fracture surfaces for PEEK samples and nacre. (A) and (B) Fracture surfaces of non-PIF and PIF-processed samples after tensile tests; (C) and (D) fracture surfaces of non-PIF and PIF-processed samples after impact tests; (E) a photo of nacre; (F) fracture surfaces of nacre; (G) a scheme of oriented stratified microstructures and the energy-dissipating paths in nacre. The cartoons above the images show the specific locations of the characterized fracture surfaces for each sample, where the right edge of each cartoon represents the fracture surface after tensile or impact tests. Note that the fracture surfaces in (B) and (D) are parallel to the upper and front surfaces of the samples, respectively.

components, leading to breakage of the material. However, for the PIF-processed samples, only a decrease in slope could be observed in the stress–strain curve at the "first yield point", and the material retained a certain percentage of stiffness and moduli until the tensile stress and strain increased to the "second yield" point and caused a break. These phenomena could be signals of internal changes in microstructures, *e.g.*, the emergence of new phase structures or new routes of deformation and slippage along phase boundaries.

It is noteworthy that the results of the PEEK system are different from the situations in many other semi-crystalline polymers, such as polypropylene, polylactic acid and polyamide, where in all curves for PIF-processed samples, an inflection occurred right at the yield point of a non-PIF sample (with the same stress and strain).[30,31,33] For PEEK samples with smaller compression ratios of 1.4 and 1.6, the initial slopes of the stress–strain curves were lower than those of the samples without PIF-processing, indicating smaller Young's moduli. We speculate that the spherulites in the PEEK system are more readily deformed under compression, as occurs in shear yielding.[34,35] Interestingly, there is similarity in the situation of the polyphenylene sulfide (PPS) system, where the modification of PIF-processing might provide a negative impact on tensile strength and impact strength under certain temperatures and pressures.[36]

The microstructural changes could be revealed by SEM observations on the fracture surfaces of samples after impact and tensile tests, where the fractural morphologies clearly presented the changes due to PIF-processing, as shown in Fig. 3. Compared to the disorderly fracture surfaces indicating brittle fracture for non-PIF samples, the samples with PIF-processing exhibited clearly oriented and stratified morphologies of overlapped layers similar to nacre (see Fig. 3E and F),[24] regardless of the loading pressure.

However, a closer look at the images showed a difference between the fracture surfaces after tensile and impact tests. As revealed by the morphologies of impact fracture surfaces (Fig. 3D), the spherulites deformed and aligned in the pressure-induced flow direction to form parallel layers no thicker than 5 μm and show a nice orientation of cracks perpendicular to LD. Meanwhile, protrusions and grooves due to the pull-out of spherulites from opposite surfaces were clearly observed along FD. We speculate that the zigzag arrangement of deformed spherulites contributed to the tortuous energy dissipating paths and resulted in improved toughness (similar to what happens in nacre, Fig. 3G), while the alignment and stretching of the amorphous regions between lamellae and spherulites are responsible for the large elongation at break. Interestingly, much narrower microsheets could be seen under high magnification within the deformed spherulites, with smaller holes and fibrous protrusions between them. The tensile fracture surface morphologies observed by SEM (Fig. 3B) demonstrate the alignment and orientation of parallel microsheets that are much thinner than deformed spherulites, with obscure

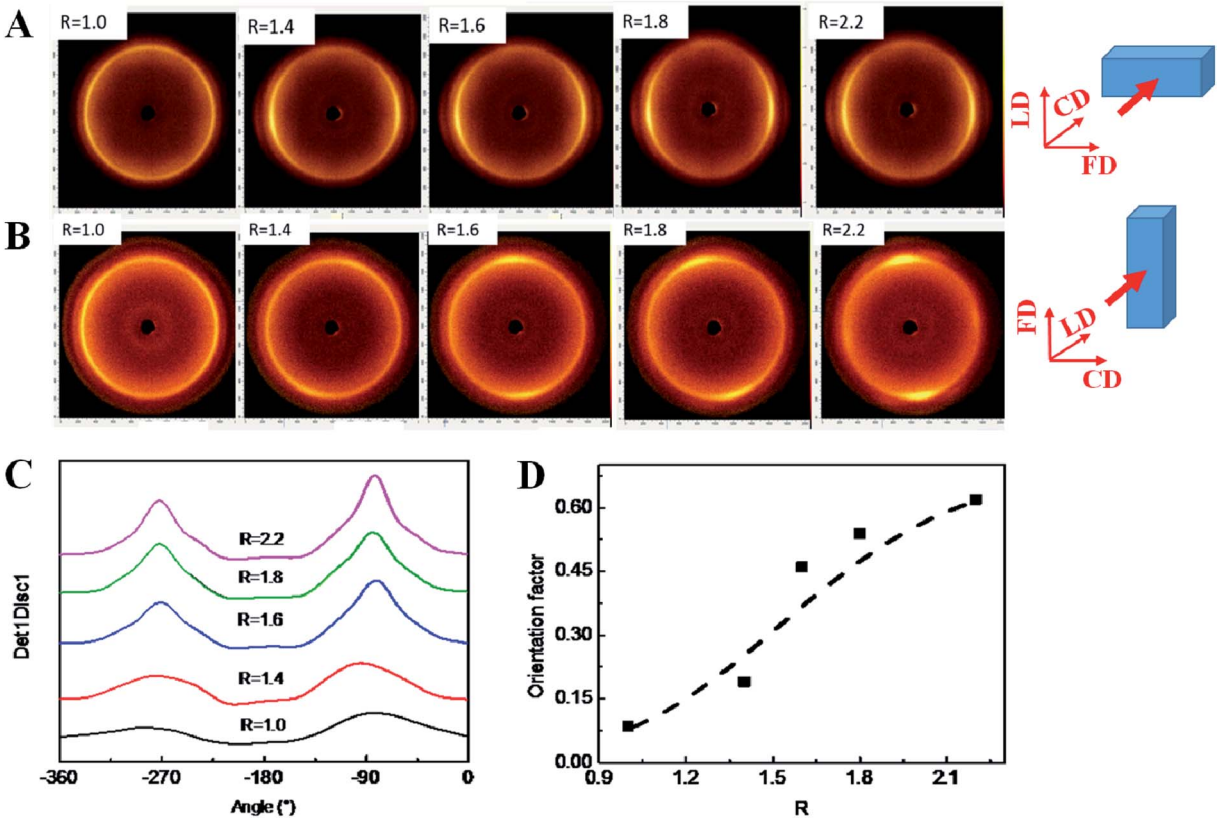

Fig. 4 2D-XRD patterns of PEEK samples: (A) CD direction; (B) LD direction. SAXS analytic curve of PEEK samples: (C) direction angle integral; (D) orientation factor.

boundaries between them. Also, holes and fibrous protrusion could be seen under high magnification, indicating a fracture mode closer to plastic deformation and ductile fracture. Upon impacting or stretching, the slippage and pull-out between those closely packed crystalline plates result in the further improvement of both the impact and tensile strength of the samples. This coincides with the research that at large deformations in uniaxial tension, PEEK undergoes molecular alignment and localization of a neck, which complicates characterization of its true-stress strain behavior up to failure.[37] The cartoons above the images show the specific locations of the characterized fracture surfaces for each sample, where the right edge of each cartoon represents the fracture surface after tensile or impact tests. It was found that non-PIF samples basically exhibit a brittle fracture, while the PIF-processed samples show a clear ductile fracture with the fracture faces somewhat propagating along FD. Hence, the fracture surfaces parallel to the upper surface of the samples and those parallel to the front surface of the samples could be picked out in Fig. 3B and D, respectively. The brittle ductile transition here, as a result of the protrusions and holes of different length scale, further confirmed the influence of PIF-processing on improving the toughness.

An unresolved problem remains is how the spherulites and lamellae could evolve into nacre-like microsheets by affine deformation or fragmentation and rearrangement of the lamellae. Crystal orientation was analysed with the aid of two-dimensional X-ray diffraction (2D-XRD), as illustrated in Fig. 4. As previously reported, polymers show better mechanical properties along the orientation direction.[38,39] The non-PIF PEEK sample ($R = 1.0$) showed homogeneous diffraction rings (Fig. 4A and B), indicating a random orientation of crystals and an isotropic microstructure. As the compression ratio increases, the diffraction rings gradually degenerate into equatorial arcs, indicating that the crystalline blocks within fibrils have a molecular orientation parallel to the crystalline-amorphous alternating direction, *i.e.*, along FD, indicating a rotation of molecular orientation from along LD to along FD. To further demonstrate the change in orientation, the XRD image is integrated to obtain the azimuth curve, as shown in Fig. 4C. The azimuth curve obtained from the PEEK sample ($R = 1.0$), without PIF molding, has no obvious peak. However, when the sample deforms under a certain pressure, an obvious peak appears in the azimuth curve, and the peak on the curve gradually becomes sharp, indicating that the degree of orientation increases. The orientation degree can be calculated according to the Hermann orientation parameter as

$$f = (3\cos^2 \Phi - 1)/2 \quad (3)$$

where f is the orientation factor and Φ is the angle between the flow direction and lamellae orientation. The above equation establishes a connection between the orientation factor and the

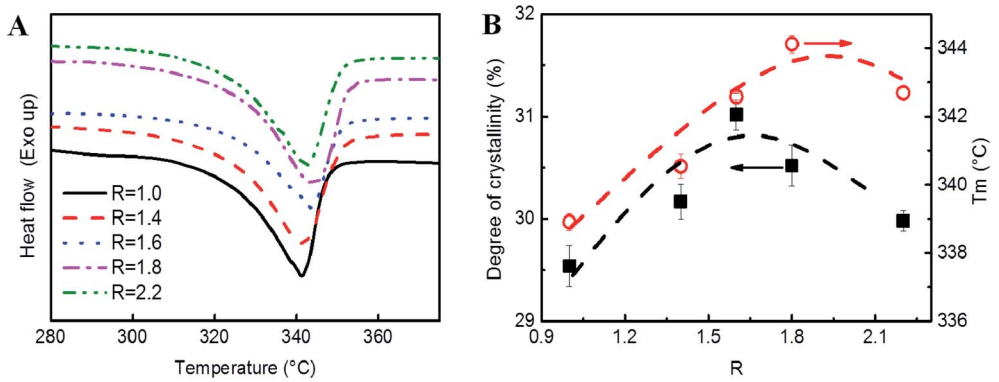

Fig. 5 (A) DSC heating curves of PEEK samples with different compression ratios; (B) crystallinity and melting temperature of PEEK samples with different compression ratios.

compression ratio and vividly demonstrates the enhanced orientation with increasing compression ratio (Fig. 4D), which reaches 0.6 under a compression ratio of 2.2. Combining similar evidences from other systems like PP, we can conclude that the microsheets in Fig. 4B and D are the results of the rotation, recombination and restacking of the crystalline blocks, which dominate the rearrangement of lamellae and the deformation of spherulites.

DSC measurements were also performed to trace any possible structural changes in the lamellae (Fig. 5). It can be concluded from the minor changes in melting point, crystallinity and the shape of melting peak that there are no obvious structural changes in the basic units for lamellae, in accordance with the above statements that the rotation, recombination and restacking of the crystalline blocks dominate the rearrangement of lamellae.

Although the nacre-like stratified structure has been clearly interpreted at this stage, the strange "second yield" and large elongation at break remain to be resolved. Changes in mechanical properties, especially those related to structural evolution in amorphous regions, can be monitored using dynamic mechanical analysis (DMA) over a range of ratios and mold temperatures. Fig. 6 presents the DMA curves of PEEK samples under different compression ratios and different molding temperatures. For Fig. 6A, the molding temperature was kept at 280 °C to evaluate the effect of different compression ratios. For Fig. 6B, the molding pressure is adjusted so that the compression ratio of all samples is approximately 1.7 to ensure the flow deformation of PEEK samples but maintain a consistent crystal orientation. As shown in Fig. 6A, the non-PIF processed exhibits only an α relaxation (glass transition) at approximately 170 °C, while the samples with PIF-processing show an additional relaxation (hereafter referred to as the PIF-relaxation) at approximately 280 °C, which is very close to the molding temperature. At the same time, the peak temperature of α relaxation (the glass transition temperature, T_g) moves to the right as the compression ratio increases. As shown in Fig. 6B, T_g remains almost constant at about 180 °C, providing a specific molding pressure, while the peak temperature of the PIF-relaxation continuously increases with the molding temperature, as further demonstrated in Fig. 6C. It is easy to conclude that for a semi-crystalline polymer with a medium degree of crystallinity, such as PEEK, the rise in T_g with the PIF-process depends mainly on the compression ratio, while the rise in peak temperature of PIF-relaxation largely relies on the molding temperature.

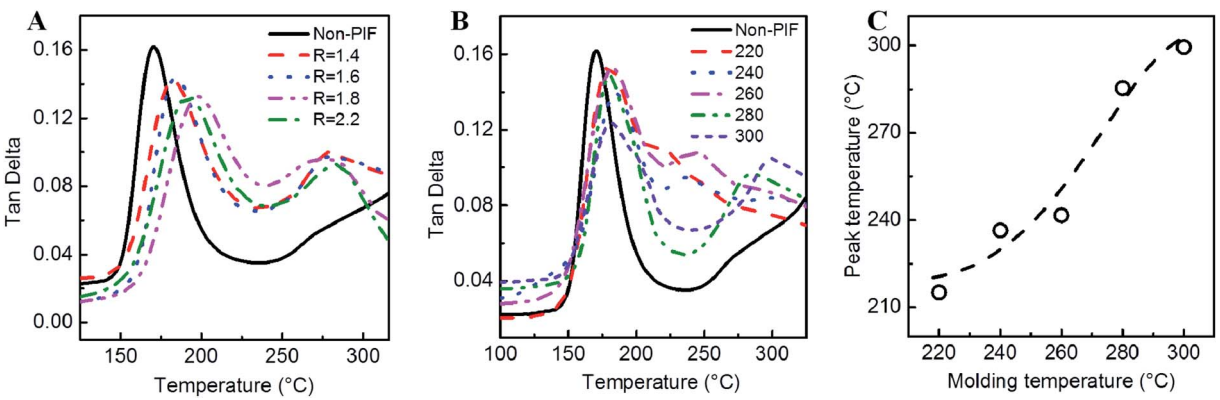

Fig. 6 DMA test curves of PEEK samples: (A) with different compression ratios at 280 °C; (B) at different molding temperatures with a constant compression ratio of 1.7; (C) relationship between the peak temperature of PIF-relaxation and the molding temperature of PIF.

No transformation similar to PIF relaxation has been reported in pure PEEK systems until now, but in research on polypropylene (PP), a large number of results have shown that crystallized PP may exhibit additional relaxation at temperatures between T_g and T_m (80–140 °C).[40] Researchers acknowledge that the addition relaxation of PP originates from the molecular movement in the crystalline zone, whereas the peak temperature and amplitude of the addition relaxation are closely related to the molecular weight, crystallinity, crystalline morphology, stereo regularity, heat treatment conditions and the existence of a swelling agent of organic small molecules. We ascribe the PIF-relaxation to the rigid amorphous fraction (RAF) around crystal lamellae,[41] which includes the tie molecules involved in the interspace between lamellae,[42] the chain loops embedded between two lamellae of spherulites,[43] the chain heads or chain tails detached from the lamella fibrils,[44] and so on. Most of these amorphous components are located in or attached to crystalline regions, and their motions are highly constrained, partly due to the spatial confinement or stretching by the crystalline phase and partly because of the inner strain within the amorphous phase itself. As a result, the relaxation of RAF is shifted to temperatures higher than T_g, and the magnitude of the temperature shift is related to the extent of confinement. The peak temperature substantially increases with increasing molding temperature, indicating that the higher mobility of molecular chains favors the conversion of lamella-adjacent amorphous components into RAF *via* the relative slippery and transverse alignment of crystal lamellae. This well accounts for the "second relaxation" in tensile curves, which appears at larger stresses. We speculate that some changes in microstructures of the materials after PIF-processing hindered the strain softening after the first yielding transition, and the orientation-induced increase in RAF, as a toughened "mortar", further boosted the improvement of the impact strength.

Regarding the α relaxation, the rise in T_g with increasing temperature and compression ratio indicates that PIF-processing also brings a confinement in normal amorphous regions. Since the temperature shift depends mainly on the compression ratio and not the molding temperature, we speculate that the reduced free volume due to flow-induced orientation and the compact stacking of molecular segments are the underlying reason. Given the limited extent of confinement in molecular mobility, an broadened area of the loss peak and a slight rise in T_g take place, instead of the large shift in peak temperature observed in PIF-relaxation. Obviously, the PIF-relaxation must be associated with certain rearrangements between chain segments, which highly rely on molecular mobility at different temperatures and produce a new phase more rigid than the amorphous region.

We speculate that the much enhanced mechanical properties might be attributed to the slippery and transverse alignment of crystal lamellae, the resultant confinement of crack propagations and the tortuous energy dissipating paths, as well as the newly formed RAF. The PIF field first leads to an elongation of the spherulites which then fragment into regions of oriented lamellae. Facilitated by the flow of the softer matrix (amorphous phase), the hard segments can slip upon each other and are finally rearranged into an ordered system containing a random and overlapping alignment of lamellae. Upon an impacting or stretching force, the delamination, the slippage and pull-out between the lamellae stacks, the plastic deformation of RAF at the interface, as well as the greatly increased sum distance of energy-dissipating paths, resulting in improvement of both impact and tensile strength of the PIF-processed samples.

It is worth noting that the tensile strength and impact strength of PIF-processed PEEK could even overtake 30% (w/w) chopped carbon fiber reinforced (CCFR) PEEK composite,[9] which has been widely used as load-bearing implants. The only hindrance lies in the Young's moduli, which are no more than that of unfilled PEEK. A combination of PIF-processing and incorporation of chopped carbon fiber seems to be able to produce a material with even better overall performance. Although the effect of PIF-processing on PEEK composites is beyond the scope of the present research, our previous investigation on CF/PPS composites confirmed that the Young's modulus could surpass the value of non-PIF samples.[36] Considering that in reality, CCFR PEEK requires additional reinforcement to achieve sufficient strength to replace conventional metallic materials,[3] we believe that PIF-processing can endow the PEEK material with improved mechanical matching with the surrounding tissues and extended service life in biomedical applications. Inspired by the PIF boosted strength and toughness, one can even reduce the volume fraction of chopped carbon fiber to obtain a balance between processability and performance.

There are still other issues to be clarified. First, PIF-processed samples should retain most of the excellent characteristics of PEEK material, including the excellent biocompatibility, because no external substances are introduced into the system. Second, the RAF and resultant nacre-like structures could be "melted" at temperatures higher than the PIF-processing temperature but well hold the integrity at room temperature. Third, the markedly increased impact strength and elongation at break benefit the use of PEEK in fields such as saccule expanding tubes and seals, especially when the ductility is emphasized. In summary, PIF-processed PEEK materials are promising candidates for broadened biomedical applications, such as various implants.

4. Conclusions

The tensile strength and impact strength for PEEK could be markedly and simultaneously improved using a processing of pressure induced flow in the solid-state. The tensile strength and impact strength could be increased to ~2 folds and ~450%, respectively. The efficiency of the enhancement could be controlled by the molding temperature and the compression ratio.

The mechanisms for the enhanced mechanical properties were proposed. The slippery and transverse alignment of crystal lamellae form an oriented and stratified nacre-like morphology that confines the resultant crack propagations as well as

tortuous energy dissipating paths. The PIF field first leads to elongation of the spherulites, followed by fragmentation into regions of oriented lamellae. Facilitated by the flow of the softer matrix (amorphous phase), the hard segments can slip upon each other and are finally rearranged into an ordered system containing a random and overlapping alignment of lamellae. Upon an impacting or stretching force, the delamination, slippage and pull-out between the lamellae stacks, plastic deformation of RAF at the interface, and greatly increased sum distance of energy-dissipating paths resulted in improvement of both the impact and tensile strength of the PIF-processed samples.

Author contributions

Conceptualization, Shu Zhu, Jianfeng Zhou; data curation, Shu Zhu, Tianwen Yan, Jianfeng Zhou and Sen Zhang; formal analysis, Tianwen Yan; funding acquisition, Shu Zhu and Jianfeng Zhou; investigation, Jianfeng Zhou, Tianwen Yan and Mengyun Xiong; methodology, Shu Zhu and Jianfeng Zhou; project administration, Jianfeng Zhou; resources, Shu Zhu; supervision, Shu Zhu; validation, Sen Zhang and Mengyun Xiong; visualization, Sen Zhang; writing – original draft, Jianfeng Zhou, Tianwen Yan and Mengyun Xiong; writing – revising & editing, Shu Zhu.

Conflicts of interest

The authors declare no conflicts of interest.

Acknowledgements

The authors would like to acknowledge the funding supported by the National Natural Science Foundation of China (52173247), the Shanghai Science and Technology Committee Project (20511107200), funding from State Key Laboratory for Modification of Chemical Fibers and Polymer Materials (KF2013, KF2012), and the Base Project of Key Laboratory of High Performance Fibers & Products in Ministry of Education (2232021G-02).

References

1 L. Ning, C. Deqiang, G. Xiyan, L. Lirong and C. Weizeng, Biological tribology properties of the modified polyether ether ketone composite materials, *Rev. Adv. Mater. Sci.*, 2020, **59**, 399–405.
2 C. Yang, J. Xu, Y. Xing, S. Hao and Z. Ren, Covalent polymer functionalized graphene oxide/poly(ether ether ketone) composites for fused deposition modeling: Improved mechanical and tribological performance, *RSC Adv.*, 2020, **10**, 25685–25695.
3 D. F. Williams, A. McNamara and R. M. Turner, Potential of polyetheretherketone (PEEK) and carbon-fiber-reinforced peek in medical applications, *J. Mater. Sci. Lett.*, 1987, **6**, 188–190.
4 K. W. Chan, C. Z. Liao, H. M. Wong, K. W. Kwok Yeung and S. C. Tjong, Preparation of polyetheretherketone composites with nanohydroxyapatite rods and carbon nanofibers having high strength, good biocompatibility and excellent thermal stability, *RSC Adv.*, 2016, **6**, 19417–19429.
5 F. Cofano, G. Di Perna, M. Monticelli, N. Marengo, M. Ajello, M. Mammi, G. Vercelli, S. Petrone, F. Tartara, F. Zenga, *et al.*, Carbon fiber reinforced vs titanium implants for fixation in spinal metastases: a comparative clinical study about safety and effectiveness of the new "carbon-strategy", *J. Clin. Neurosci.*, 2020, **75**, 106–111.
6 H. B. Skinner, Composite technology for total hip-arthroplasty, *Clin. Orthop. Relat. Res.*, 1988, **235**, 224–236.
7 B. Wang, K. Zhang, C. Zhou, M. Ren, Y. Gu and T. Li, Engineering the mechanical properties of CNT/PEEK nanocomposites, *RSC Adv.*, 2019, **9**, 12836–12845.
8 S. Mishra and R. Chowdhary, PEEK materials as an alternative to titanium in dental implants: a systematic review, *Clinical Implant Dentistry and Related Research*, 2019, **21**, 208–222.
9 S. M. Kurtz and J. N. Devine, PEEK biomaterials in trauma, orthopedic, and spinal implants, *Biomaterials*, 2007, **28**, 4845–4869.
10 S. Schroeder, S. Braun, U. Mueller, M. Vogel, R. Sonntag, S. Jaeger and J. P. Kretzer, Carbon-fibre-reinforced PEEK: an alternative material for flexion bushings of rotating hinged knee joints?, *J. Mech. Behav. Biomed. Mater.*, 2020, **101**, 103434.
11 G. F. Vles, M. H. Brodermann, M. A. Roussot and J. Youngman, Carbon-fiber-reinforced PEEK intramedullary nails defining the niche, *Case Rep. Orthoped.*, 2019, **2019**, 1538158.
12 S. L. Evans and P. J. Gregson, Composite technology in load-bearing orthopaedic implants, *Biomaterials*, 1998, **19**, 1329–1342.
13 J. Ma, Q. Liang, W. Qin, P. O. Lartey, Y. Li and X. Feng, Bioactivity of nitric acid and calcium chloride treated carbon-fibers reinforced polyetheretherketone for dental implant, *J. Mech. Behav. Biomed. Mater.*, 2020, **102**, 103497.
14 R. O. Ritchie, The conflicts between strength and toughness, *Nat. Mater.*, 2011, **10**, 817–822.
15 *A high stiffness PEEK grade*, 26 May 2014, **https://www.jeccomposites.com/knowledge/international-composites-news/high-stiffness-peek-grade**.
16 P. Liu, Y. Zhong, Q.-X. Pei, V. Sorkin and Y.-W. Zhang, Simultaneously enhancing the strength and toughness of short fiber reinforced thermoplastic composites by fiber cross-linking, *Compos. Sci. Technol.*, 2022, **217**, 109076.
17 A. P. Jackson, J. F. V. Vincent and R. M. Turner, The mechanical design of nacre, *Proc. R. Soc. B*, 1988, **234**, 415–440.
18 F. Barthelat, H. Tang, P. D. Zavattieri, C. M. Li and H. D. Espinosa, On the mechanics of mother-of-pearl: a key feature in the material hierarchical structure, *J. Mech. Phys. Solids*, 2007, **55**, 306–337.

19 J. Sun and B. Bhushan, Hierarchical structure and mechanical properties of nacre: a review, *RSC Adv.*, 2012, **2**, 7617–7632.
20 F. Barthelat, Designing nacre-like materials for simultaneous stiffness, strength and toughness: optimum materials, composition, microstructure and size, *J. Mech. Phys. Solids*, 2014, **73**, 22–37.
21 S. Morsali, D. Qian and M. Minary-Jolandan, Designing bioinspired brick-and-mortar composites using machine learning and statistical learning, *Commun. Mater.*, 2020, **1**, 2662–4443.
22 M. Q. Sun, P. Shen and Q. C. Jiang, Microstructures and mechanical characterizations of high-performance nacre-inspired Al/Al_2O_3 composites, *Composites, Part A*, 2019, **121**, 465–473.
23 L. Adler-Abramovich, Z. A. Arnon, X. M. Sui, I. Azuri, H. Cohen, O. Hod, L. Kronik, L. J. W. Shimon, H. D. Wagner and E. Gazit, Bioinspired flexible and tough layered peptide crystals, *Adv. Mater.*, 2018, **30**, 1704551.
24 A. Finnemore, P. Cunha, T. Shean, S. Vignolini, S. Guldin, M. Oyen and U. Steiner, Biomimetic layer-by-layer assembly of artificial nacre, *Nat. Commun.*, 2012, **3**, 966.
25 Y.-L. Li, R.-F. Guo, Z.-J. Hu and P. Shen, Construction of nacre-mimetic composites with a "brick-and-mortar" architecture based on structural defects in ice-templating, *Mater. Des.*, 2021, **204**, 109668.
26 L. Jin, M. Zhang, L. Shang, L. Liu, M. Li and Y. Ao, A nature-inspired interface design strategy of carbon fiber composites by growing brick-and-mortar structure on carbon fiber, *Compos. Sci. Technol.*, 2020, **200**, 108382.
27 J. Peng, A. P. Tomsia, L. Jiang, B. Z. Tang and Q. Cheng, Stiff and tough pdms-mmt layered nanocomposites visualized by aie luminogens, *Nat. Commun.*, 2021, **12**, 4539.
28 P. Podsiadlo, A. K. Kaushik, E. M. Arruda, A. M. Waas, B. S. Shim, J. Xu, H. Nandivada, B. G. Pumplin, J. Lahann, A. Ramamoorthy, *et al.*, Ultrastrong and stiff layered polymer nanocomposites, *Science*, 2007, **318**, 80–83.
29 Z. Qin, X. Ren, L. Shan, H. Guo, C. Geng, G. Zhang, S. Ji and Y. Liang, Nacre like-structured multilayered polyelectrolyte/calcium carbonate nanocomposite membrane via Ca-incorporated layer-by-layer-assembly and CO_2-induced biomineralization, *J. Membr. Sci.*, 2016, **498**, 180–191.
30 S. Zhu, K. Han, S. Zhang, Z. Jiang, Q. Huan, Y. Ma and M. Yu, Simultaneously boosting toughness and tensile strength for polyamide 6/montmorillonite nanocomposite by a pressure-induced flow field, *J. Macromol. Sci., Part B: Phys.*, 2014, **53**, 1601–1608.
31 Q. Huan, S. Zhu, Y. Ma, J. Zhang, S. Zhang, X. Feng, K. Han and M. Yu, Markedly improving mechanical properties for isotactic polypropylene with large-size spherulites by pressure-induced flow processing, *Polymer*, 2013, **54**, 1177–1183.
32 L. Z. Zhang and M. Li, Study on properties of PEEK composites reinforced by SCF, *Adv. Mater. Res.*, 2012, **476–478**, 705–709.
33 S. Zhang, X. Feng, S. Zhu, Q. Huan, K. Han, Y. Ma and M. Yu, Novel toughening mechanism for polylactic acid (PLA)/starch blends with layer-like microstructure via pressure-induced flow (PIF) processing, *Mater. Lett.*, 2013, **98**, 238–241.
34 W. Hu, *Polymer physics: a molecular approach*, Springer-Verlag, Wien, Heidelberg, New York, Dordrecht, London, 2013.
35 Y. Wang, Z. Jiang, Z. Wu and Y. Men, Tensile deformation of polybutene-1 with stable form I at elevated temperature, *Macromolecules*, 2013, **46**, 518–522.
36 Y. Xu, S. Zhu, Z. Zhang, M. Yu and X. Yuan, A new way of strengthening and toughening for carbon fiber reinforced polyphenylene sulfide (CF/PPS) composites via matrix modification, *J. Wuhan Univ. Technol., Mater. Sci. Ed.*, 2017, **32**, 1318–1322.
37 P. J. Rae, E. N. Brown and E. B. Orler, The mechanical properties of poly(ether-ether-ketone) (PEEK) with emphasis on the large compressive strain response, *Polymer*, 2007, **48**, 598–615.
38 B. Dillon, P. Doran, E. Fuenmayor, A. V. Healy, N. M. Gately, I. Major and J. G. Lyons, Influence of annealing and biaxial expansion on the properties of poly(l-lactic acid) medical tubing, *Polymers*, 2019, **11**, 1172.
39 M. Á. Caminero, J. M. Chacón, E. García-Plaza, P. J. Núñez, J. M. Reverte and J. P. Becar, Additive manufacturing of pla-based composites using fused filament fabrication: effect of graphene nanoplatelet reinforcement on mechanical properties, dimensional accuracy and texture, *Polymers*, 2019, **11**, 799.
40 I. Inamura, H. Ochiai and H. Yamamura, Effects of swelling and annealing on the viscoelastic behavior of solution-crystallized and melt-crystallized samples of fractionated polypropylene, *J. Polym. Sci., Polym. Phys. Ed.*, 1976, **14**, 1221–1234.
41 B. Wunderlich, Reversible crystallization and the rigid-amorphous phase in semicrystalline macromolecules, *Prog. Polym. Sci.*, 2003, **28**, 383–450.
42 J. H. Weiner and D. H. Berman, Thermomechanical behavior of interacting tie molecules in semicrystalline polymers, *Macromolecules*, 1984, **17**, 2015–2018.
43 R. Seguela, Critical review of the molecular topology of semicrystalline polymers: the origin and assessment of intercrystalline tie molecules and chain entanglements, *J. Polym. Sci., Part B: Polym. Phys.*, 2005, **43**, 1729–1748.
44 M. Ishikawa, K. Ushui, Y. Kondo, K. Hatada and S. Gima, Effect of tie molecules on the craze strength of polypropylene, *Polymer*, 1996, **37**, 5375–5379.